RSC Advances

PAPER

Cite this: *RSC Adv.*, 2016, **6**, 105699

m-Cresol affects the lipid bilayer in membrane models and living neurons†

T. O. Paiva,‡[a] A. E. P. Bastos,‡[ab] J. T. Marquês,[a] A. S. Viana,[a] P. A. Lima[b] and R. F. M. de Almeida*[a]

m-Cresol is a preservative used in pharmaceutical formulations, including insulin and vaccines, which contain up to 30 millimolar concentrations of this excipient. We studied the effects of *m*-cresol (from 1 : 1 to 1 : 10^4 dilution relative to the formulations) on membrane model systems containing liquid ordered domains, alone or in an insulin formulation. These studies allowed to understand the effects of this compound on cell membranes when present in pharmaceutical formulations, and to explain its cytotoxic effects. Changes in the intrinsic fluorescence of *m*-cresol showed a clear interaction with liposomes that depends on their lipid composition. Liposomes labeled with several membrane probes revealed the superficial location of *m*-cresol, alone and within insulin formulation, with an unusual preference for liquid ordered cholesterol–sphingolipid-enriched domains due to their high membrane dipole potential. Membrane probes detected the effects of *m*-cresol at a concentration of 1 : 10 000 relative to the original formulations. Atomic force microscopy imaging of ternary supported lipid bilayers allowed the observation that addition of *m*-cresol affects precisely the ordered raft-like nanodomains, with a fast (5 min) effect at 1 : 10 dilution that became massive after 1 h. When contained in insulin formulation, similar *m*-cresol effects were observed. To evaluate the importance of the direct interactions of *m*-cresol with membrane lipids at the cellular level, membrane leakage was monitored in three neuronal cell lines. *m*-Cresol was applied during constant superfusion and leak current alterations were followed. The leak conductance in living neurons underwent a dose-dependent increase. The effects reported here are likely to underlie the mechanisms of *m*-cresol toxicity for cells and tissues at or near the injection site.

Received 12th August 2016
Accepted 7th October 2016

DOI: 10.1039/c6ra20337j

www.rsc.org/advances

Introduction

Cresol was identified for the first time in 1851 and the three cresol isomers (*o*-, *m*- and *p*-cresol) in 1896.[1] Currently, they are used in different areas, such as in textile industries, as bactericides and fungicides in agriculture, in the cosmetics industry as antiseptics and fragrances, as industrial solvents in synthetic processes, in the pharmaceutical industry and in many other industries around the world.[1–3] Naturally, they are formed as metabolites from enzymatic oxidation of toluene[2] and menthofuran[3] and are components of foods and drinks, being widely disseminated in nature.[1] For that reason, its toxicity has deserved great attention and there are several toxicity studies reporting quite a lot of side effects caused by exposure to cresol.[2–5] These effects include severe inflammation of mucous membranes and hepatic injury that leads to death.[6] The toxicity has been well described for the three isomers and usually *p*-cresol is considered the most toxic isomer and its toxicity implicates the formation of reactive intermediates,[2] like reactive oxygen species, contributing to atherosclerosis and thrombosis.[3] Despite that, the degree of cell killing observed using rat liver slices in the presence of *p*-cresol can be achieved using a 5- to 10-fold higher concentration of either *o*- or *m*-cresol. Moreover, the oral LD50 of *m*-cresol is 242 mg kg^{-1},[7] similar to the other isomers,[2] and *m*-cresol was determined by the Environmental Protection Agency from the U.S. Department of Health and Human Services to be a possible human carcinogen.[8]

Dentistry is another field of application of cresols.[3,9] In conjugation with formaldehyde, they have been used in the production of dentistry products, as a component of dental materials and devices, as a solvent and as a disinfectant. Therefore, exposure to formocresol *via* inhalation has been a subject of special concern regarding its mutagenic and carcinogenic potential, as well as possible damage of the central nervous system,[10–12] like the neurotoxic effects recently reported.[13] According to these studies, lipid peroxidation

[a]*Centro de Química e Bioquímica, DQB, Faculdade de Ciências da Universidade de Lisboa, Campo Grande, Ed. C8, 1749-016 Lisboa, Portugal. E-mail: rfalmeida@fc.ul.pt; Fax: +351 2175500088; Tel: +351 217500925*

[b]*NOVA Medical School, Faculdade de Ciências Médicas da Universidade Nova de Lisboa, Campo Mártires da Pátria, 1169-056 Lisboa, Portugal*

† Electronic supplementary information (ESI) available: Fig. S1–S4. See DOI: 10.1039/c6ra20337j

‡ These authors contributed equally.

increases after exposure to cresols as a consequence of free radical production, which may induce changes in membrane fluidity and permeability.[11]

Given the ability of phenolic compounds, especially cresols, to act as antiseptics and stabilisers of protein aggregation,[14] they have been widely used in commercial pharmaceutical formulations.[15,16] Firstly, they were described as preservatives in insulin formulations,[16] used to prevent bacterial growth and to stabilize insulin molecules during storage and transport.[17] More recently, *m*-cresol and other phenolic derivatives were globally described as excipients,[18] used mainly with the intent of preserving the hexameric form of insulin and maintaining the sterility of the solution. Despite the known problematic toxic effects, cresols are used in substantial amounts in these formulations. One example is Humulin®, which contains *m*-cresol at 2.5 mg mL^{-1} and human insulin at 100 U mL^{-1} (Eli Lilly and Company), which represents *ca.* 38-fold higher concentration of *m*-cresol, corresponding to a molar concentration of 23 mM. Humulin® is a human insulin injection formulation synthesized through rDNA technology and is prescribed to improve glycemic control in patients with type 1 and type 2 diabetes mellitus, usually administrated through doses in the 0.05 to 0.4 units per kg range. It also contains glycerin at 16 mg mL^{-1}, endogenous zinc (approximately 0.015 mg/100 U) and water. Some of its side effects include swelling of the hands and feet and heart failure. The most common problem concerning insulin perfusion pumps like Humulin® are complications associated with continuous subcutaneous insulin infusion. These complications involve skin irritation and local inflammation at the infusion site and seem to be associated with the presence of *m*-cresol in large amounts, through an interference with the body's defence mechanisms.[5] In fact, patients who used an insulin formulation containing *m*-cresol had a significantly higher inflammation rate than those who used insulin with methyl *p*-hydroxylbenzoate.[4] However, comparing pure *m*-cresol with insulin formulations containing *m*-cresol, the level of toxicity was similar and even a short exposure to *m*-cresol induces cell death, whereas the insulin solution without excipients did not cause cell death.[18]

The physical properties of *m*-cresol are well described[19] and its interaction with synthetic phospholipid liposomes was studied for the first time by differential scanning calorimetry.[9] It was shown that *m*-cresol is capable of inducing changes in the phase transition temperature and the enthalpy of the transition from gel to liquid-crystalline phase. However, the effects of *m*-cresol concerning cell membranes are not well established and there is a lack of information about its fluorescence properties. Importantly, little is known about the possible functional/mechanistic effects at the cellular-membrane level. Thus, the purpose of this work is to present a detailed biophysical characterisation of the interaction between *m*-cresol and lipid bilayers in order to understand the potential effects of this compound on cell membranes. Humulin® was used as an example of a formulation containing considerable amounts of this excipient. Its fluorescence properties were evaluated in the presence of large unilamellar vesicles (LUV) formed by well characterized binary mixtures, and ternary mixtures of the low main-transition temperature/high main-transition temperature/cholesterol (Chol) type, which gives rise to the formation of sphingomyelin/Chol-enriched domains, mimicking the outer leaflet of mammalian plasma membranes.[20] Using atomic force microscopy (AFM) with supported lipid bilayers (SLB), the effects of *m*-cresol and Humulin® were evaluated in real-time. The concentration of *m*-cresol reaches 30 mM in some insulin formulations and therefore serial 1 : 10 dilutions were studied, as in recent cytotoxicity studies,[18] to understand the effects on cell membranes at the site of application, and in cells and tissues away from that site. The chemical structures of *m*-cresol and the lipid molecules used in this work are represented in Fig. 1. 1-Palmitoyl-2-dioleoyl-*sn-glycero*-3-phosphocholine (POPC) is one of the most abundant glycerophospholipids of eukaryotic organisms' cell membranes, while sphingomyelin, in this work represented by *N*-palmitoyl-sphingomyelin (PSM), is the sphingolipid that exists in higher amounts in animal cell membranes and Chol is their central sterol.[21] The functional relevance of *m*-cresol was studied by whole-cell voltage clamp recordings in three neuronal cell types: a neuroblastoma cell line (N1E-115), neurons from the peripheral nervous system (dorsal root ganglia (DRG) neurons) and neurons from the central nervous system (hippocampal neurons). In all, a dose dependent effect was detected on the leakage current, showing that *m*-cresol alters neural membrane integrity.

Materials and methods

Chemicals

1,2-Dioleoyl-*sn-glycero*-3-phosphocholine (DOPC), POPC, PSM and *N*-(lissamine rhodamine B sulfonyl)-1,2-dioleoyl-*sn-glycero*-3-phosphoethanolamine ammonium salt (Rhod-DOPE) were purchased from Avanti Polar Lipids (Alabaster, AL); bovine insulin, Chol, minimum 99%, and Ludox (colloidal silica diluted to 50 wt% in water) were purchased from Sigma-Aldrich (Barcelona, Spain). *trans*-Parinaric acid (*t*-PnA), *N*-(7-nitrobenz-2-oxa-1,3-diazol-4-yl)-1,2-dipalmitoyl-*sn-glycero*-3-phosphoethanolamine triethylammonium salt (NBD-DPPE) and *N*-(7-nitrobenz-2-oxa-1,3-diazol-4-yl)-1,2-dioleoyl-*sn-glycero*-3-phosphoethanolamine (NBD-DOPE) were purchased from Invitrogen (Madrid, Spain). *m*-Cresol was obtained from MERCK

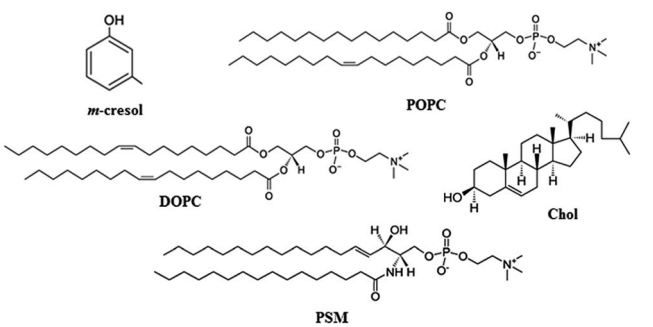

Fig. 1 Structural formulae of *m*-cresol and the lipid molecules used in this work.

(Germany) and Humulin® REGULAR 100 UI mL^{-1} from Lilly Lda. (Portugal), containing *m*-cresol 2.5 mg mL^{-1}. Other reagents were of the highest purity available. Two buffers were used for hydration of lipid mixtures: (i) 10 mM Hepes, 150 mM NaCl, pH 7.4 (HEPES buffer); (ii) 2.70 mM K_2HPO_4, 1.50 mM NaH_2PO_4, 150 mM NaCl, pH 7.4 (PBS).

Phospholipid, cholesterol, *m*-cresol and fluorescent probes quantification

The phospholipid concentration was determined gravimetrically and by inorganic phosphate quantification.[22] Cholesterol quantification was achieved by gravimetry. *m*-Cresol concentration was determined spectrophotometrically using ε (270 nm) = 2.34 M^{-1} cm^{-1}.[23] Probe concentrations in stock solutions (spectroscopic grade solvents) were determined spectrophotometrically using ε (NBD-DPPE or DOPE, 465 nm, chloroform) = 21 × 10^3 M^{-1} cm^{-1}; ε (Rhod-DOPE, 559 nm, chloroform) = 95 × 10^3 M^{-1} cm^{-1}; and ε (*t*-PnA, 299.4 nm, ethanol) = 89 × 10^3 M^{-1} cm^{-1}.[24]

Lipid mixtures and multilamellar vesicles (MLV) preparation

In the fluorescence spectroscopy studies, 4 different systems were used (POPC/PSM/Chol, POPC/Chol, POPC/PSM, and DOPC/PSM/Chol). For the POPC/PSM/Chol system, the following molar proportions of each lipid component were prepared: 80/20/0, 71.8/23.1/5.1, 60/26/14, 48.5/29.3/22.2, 33.3/33.3/33.3 and 25.2/35.5/39.3. These compositions were selected to span the tie line containing the 1 : 1 : 1 equimolar mixture, taken from the ternary phase diagram.[20] For the POPC/Chol system, the molar proportions of each component were 100/0, 94.9/5.1, 86/14, 77.8/22.2, 66.7/33.3 and 60.7/39.3, and for POPC/PSM were 100/0, 80/20, 70/30, 60/40, 50/50, 40/60, 30/70, 20/80 and 0/100. In the AFM studies, the ternary mixture of DOPC/PSM/Chol (40/40/20 mol/mol/mol), also studied by fluorescence spectroscopy, was employed. Lipid stock solutions and lipid mixtures were prepared with spectroscopic grade chloroform. The solvent was slowly evaporated under a mild flow of nitrogen, followed by overnight vacuum. MLV suspensions were prepared by hydration of the mixtures with either HEPES buffer for small unilamellar vesicles (SUV) and SLB preparation, or PBS for LUV preparation, and progressively suspended by vortex stirring and freeze–thaw cycles (T > 50 °C).

SLB preparation and interaction with *m*-cresol

SUV (total lipid concentration 1 mM) were obtained by power sonication (Hielscher, UP200S). 150 μL of the resulting suspension with 5 mM $CaCl_2$ was deposited on freshly cleaved mica (Veeco) and incubated for 1 h at 60 °C. After this incubation step, the SLB samples were left at room temperature for 1 h to cool and then washed several times with HEPES buffer.[25] The SLB samples were initially covered with 80 μL of HEPES buffer. After AFM imaging in a region of interest, successive additions of higher concentrations of *m*-cresol and Humulin® were performed with at least 2 h between each one. The same region was imaged several times between and after each addition of *m*-cresol and Humulin®. Successive additions of HEPES buffer and insulin were also performed as a control.

AFM imaging

In situ AFM measurements were performed at room temperature using a Multimode Nanoscope IIIa microscope (Digital Instruments, Veeco). Topographic images were taken with a scan rate of *ca.* 2 Hz in tapping mode. Before each experiment, the glass block holding the cantilever was washed several times with water and ethanol. The cantilevers used were made of silicon nitride (NPS, *ca.* 0.58 N m^{-1} of spring constant, Veeco) with a resonance frequency in liquid of about 9 kHz. In many cases, regions with small defects and where the lipid domains had distinctive shapes were chosen, in order to easily identify the changes in lateral organization of the membrane. The images presented in this study are representative of each sample (the observations are uniform for the whole sample); at least 3 independent experiments on freshly prepared SLB have been performed. To obtain the thickness values (or thickness differences) for each sample, at least 10 different topographic profiles were drawn, and the median value taken. The most representative profiles were selected for the figures shown. The relative area corresponding to the different types of domains in each image was calculated using the software ImageJ.

LUV preparation and interaction with *m*-cresol

LUV (total lipid concentration 1 mM) were prepared by standard procedures.[26] LUV with *ca.* 100 nm diameter[27] were formed by extrusion (Avanti Mini-Extruder) at 60 °C, by forcing the MLV suspension 21 times through polycarbonate filters with a pore diameter of 100 nm (Nucleopore, Whatman). The probe/lipid ratio used was 1 : 500 (mol : mol) for *t*-PnA, 1 : 1000 for NBD-DOPE and NBD-DPPE and 1 : 200 for Rhod-DOPE. All probes, except *t*-PnA, were incorporated in lipid mixtures with lipid stock solutions. After extrusion, samples were kept overnight at 4 °C, protected from light. Before the measurements, samples were slowly brought to room temperature and incubated with pure *m*-cresol at 3, 30 and 300 μM or Humulin® containing *m*-cresol at 100 μM and 1 mM, at least 1 h before. In control experiments, measurements were performed with and without the presence of *m*-cresol, Humulin® and insulin.

Fluorescence spectroscopy measurements

Fluorescence intensity (I) measurements were performed at room temperature (24 ± 1 °C) in PBS solution using 1.0 cm × 0.4 cm quartz cuvettes using a Spex Fluorolog 3-22 spectrofluorometer (Horiba Jobin Yvon) equipped with double grating monochromators in both excitation and emission light paths. For steady-state measurements, the respective excitation and emission wavelengths were 275 nm and 303 nm for *m*-cresol and Humulin®, 303 nm and 405 nm for *t*-Pna, and 468 nm and 536 nm for NBD-DPPE and NBD-DOPE. The steady-state anisotropy (r) was calculated according to eqn (1).[28]

$$r = (I_{VV} - G \times I_{VH})(I_{VV} + 2G \times I_{VH}) \quad (1)$$

in which G is the instrumental correction factor. Subscripts V and H represent the vertical and horizontal orientations of the polarizers, and the order of the subscripts corresponds to

excitation and emission. An adequate blank was subtracted from each intensity reading. The set of 4 intensity components for each sample was measured 7 times. The fluorescence intensity decays were obtained by the single photon counting technique using a nanoLED N-320 (Horiba Jobin-Yvon) for the excitation of *t*-Pna and the emission wavelength was 405 nm. For the excitation of NBD-DPPE and NBD-DOPE, Nano-LED N-460 was used and the emission wavelength was 536 nm. Ludox scattering was used to obtain the instrumental response function and the background (obtained with the blank sample) was subtracted from the decay. Data analysis was performed using the software TRFA v1.4 (Scientific Software Technologies Center, Minsk, Belarus). Fluorescence intensity decays were analysed by fitting a sum of exponentials as shown in eqn (2),

$$I(t) = \sum_{i=1}^{n} \alpha_i \exp(-t/\tau_i) \quad (2)$$

where α_i and τ_i are the normalized amplitude and lifetime of the component i, respectively. The mean intensity-weighted fluorescence lifetime $\langle\tau\rangle$ was obtained through eqn (3),

$$\langle\tau\rangle = \sum(\alpha_i\tau_i^2)/\sum\alpha_i\tau_i \quad (3)$$

The quality of the fit was judged by a reduced χ^2 value close to 1 and random distribution of weighted residuals and residuals autocorrelation. All the data represents the mean ± standard deviation of at least 3 independent samples.

FRET measurements

The NBD-DPPE/Rhod-DOPE (Donor (D)/Acceptor (A)) pair with lipid ratio 1 : 1000/1 : 200 was chosen for FRET between l_o and l_d phases.[29] FRET efficiency, E, was obtained for each sample from the time-resolved fluorescence intensity curves through eqn (4),

$$E = 1 - (\bar{\tau}_{DA}/\bar{\tau}_D) \quad (4)$$

where $\bar{\tau}$ is the amplitude-weighted fluorescence lifetime of the probe in the presence of the donor only ($\bar{\tau}_D$) and with both donor and acceptor ($\bar{\tau}_{DA}$).

Whole-cell voltage clamp

Electrophysiological recordings were made from 3 different neural preparations (see below). All the procedures involving animal subjects, namely neuron and brain preparations, were performed upon approval by the Ethical Committee of the Nova Medical School from NOVA University, and according to the European and Portuguese guidelines for the protection of animals used for scientific purposes (European Union Directive 2010/63/EU, transposed to Portuguese Legislation by the Decree DL 113/2013). Whole-cell voltage-clamp recordings were made from isolated uncoupled cells at room temperature using an Axopatch 200B (Axon Instruments, Inc). Microelectrodes (1.2–3.5 MΩ) were pulled from borosilicate glass (Science Products GMBH) and filled with solution containing (in mM): $KMeSO_4$ (140) (or KF, 140, for the DRG neurons), $MgCl_2$ (1), HEPES (10), EGTA (10), $CaCl_2$ (1), Na_2ATP (2), Na-GTP (0.4); pH 7.2–7.3 titrated with KOH; calculated free $[Ca^{2+}] = 60$ nM by Webmaxclite v1.15, MaxChelator. External bathing solution was constantly superfused (~2–3 mL min^{-1}). It contained (in mM): NaCl (135) (140, for DRG neurons), KCl (5.4) (4, for DRG neurons), $CaCl_2$ (2), $MgCl_2$ (1.5), HEPES (10), D-glucose (25) (10, for DRG neurons); pH 7.4 titrated with NaOH. Currents were measured with or without cell capacitance compensation and series resistance compensation (80%), filtered at 2 kHz and sampled at 5 kHz, using a Digidata 1200 ADC converter (Axon Instruments) and pClamp software (v6).

Isolated hippocampal neurons. Pyramidal cells from the CA1 region of the hippocampus from P21 to P30 Wistar rats were isolated as described previously.[30] Briefly, rats were sacrificed by cervical dislocation followed by rapid decapitation. Brains were rapidly removed and transferred to an ice-cold solution. Subslices of the CA1 region were incubated in an oxygen-saturated solution (dissociation solution), containing (in mM) NaCl (120), KCl (5), $CaCl_2$ (1), $MgCl_2$ (1), PIPES (20), D-glucose (25) and trypsin (1 mg mL^{-1}; pH 7.2 at 32 °C), for 25–35 min. After the enzymatic treatment, the preparation was maintained in trypsin-free solution at room temperature for up to 8 h. Prior to each essay, cells were isolated by gentle mechanical titration and consequently plated in cell culture Petri dishes (p35), which were also used as recording chambers.

Isolated dorsal-ganglia neurons. Wistar rats (120–140 g) were sacrificed with pentobarbital (100 mg kg^{-1} i.p.), followed by decapitation. The DRG harvesting procedure was performed similarly to that described by Malin *et al.*[31] The DRG ganglia from L4 to L6 were removed, dissected out and placed in cold dissociation solution (same as for hippocampal neurons). Soon after, ganglia were trimmed into three pieces and incubated for 45 min at 32 °C in 3 mg mL^{-1} collagenase (type IA, Sigma C9891), prepared in dissociation solution. Pieces of DRG ganglia were mechanically dissociated with a fire-polished Pasteur pipette after 20 min and after 45 min. Trypsin (Sigma T9201) was added to the previous solution to a final concentration of 2.5 mg mL^{-1} and digestion was prolonged for a further 40 min. After digestion, an additional mechanical trituration was performed and the cell suspension was centrifuged for 5 min at 2000 rpm at room temperature. Dissociated DRG neurons were plated in poly-L-lysine-coated p35 plates containing culture medium (DMEM (Gibco) + 10% FBS + 0.1% penicillin/streptomycin). Cells were incubated at 37 °C and 5% CO_2 in air, for at least 8 h prior to whole-cell voltage-clamp experiments.

Neuroblastoma cells. N1E-115 cells (ECACC, 88112303), isolated from the adrenergic clone of the neuroblastoma C-1300 (a mouse neuroblastoma with sympathetic origin), were grown at 37 °C and 5% CO_2 in air. The DMEM (Gibco) culture medium was supplemented with 10% fetal calf serum and 0.1% penicillin/streptomycin. Cells were split weekly when confluent and were plated in 35 mm dishes (NUNC) for induction of differentiation, using medium with reduced serum content (2.5%) plus DMSO (1.5%) (differentiation medium (DM)). Cells stopped dividing and started differentiating within 1–2 days in

DM. For this study, only cells with 6 to 9 days in DM were used, as those showed clear neuritic processes.

Experimental procedure and data analysis. *m*-Cresol was applied during constant superfusion (2/3 mL min^{-1}) and the following parameters were monitored: series-resistance, whole-cell capacitance, and holding-current ($V_m = -70$ mV), which gives a measure of the leak current. An additional protocol was used as another read-out for the leak-current (Fig. 2). Two different voltage-clamp protocols were applied. Sets of incremental depolarizing commands (10 mV steps) were used for the characterisation of the voltage dependence of activation of voltage activated currents. Preceding such steps, leakage current was estimated *a posteriori* from the current–voltage relation (*I*/*V*) generated by a set of 12 or 14 prepulses in increments of 1 mV from −75 mV. Such a 1 mV step protocol resulted in a range of potentials which do not evoke any 'physiological current'; thus, the corresponding *I*/*V* showed almost linear relationships that were used to estimate the leakage current. Whole-cell data were analysed using Clampfit (v9) (Axon Instruments, Inc.) and Origin (v5) (Microcal Origin).

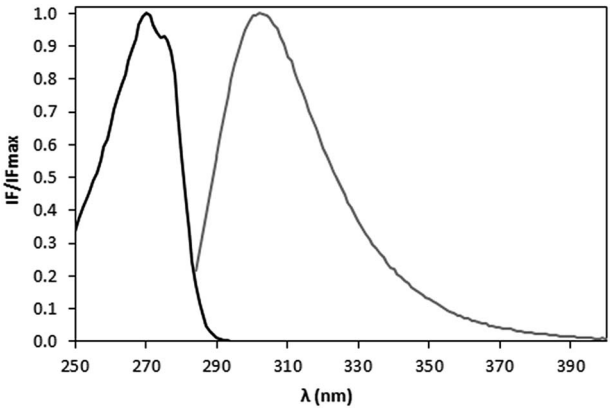

Fig. 3 Normalized excitation (black line) and emission (grey line) spectra of 30 μM *m*-cresol in PBS solution at room temperature. The represented spectra are the median of at least 3 independent experiments.

Results

Interactions of *m*-cresol with biomembranes evaluated through intrinsic fluorescence properties of *m*-cresol and insulin

m-Cresol interactions with lipid bilayers mimicking the outer leaflet of mammalian plasma membranes were evaluated through its intrinsic fluorescence properties. The maximum fluorescence excitation of *m*-Cresol occurs at 270 nm and the maximum of fluorescence emission at 302 nm (Fig. 3). The excitation and emission spectra measured are in agreement with previously reported data.[32]

This excipient is a phenol derivative[1] and displays absorption and emission in the UV region of the electromagnetic spectrum,[32] similarly to other phenol derivatives such as the aromatic amino acid tyrosine. Thus, we used this feature of *m*-cresol to directly assess its adsorption to lipid bilayers and its consequences, without the need of using external probes and still taking advantage of the high sensitivity of fluorescence spectroscopy. The molar proportions of the mixtures of POPC/PSM/Chol were chosen to span the tie-line that contains the mixture 1 : 1 : 1 on the ternary phase diagram,[20] which represents the lipid composition of the mammalian cell plasma-membrane outer leaflet.[33] Using these proportions, the effects of *m*-cresol were evaluated in the presence of a liquid ordered (l_o) and a liquid disordered phase (l_d) and in coexistence of both, since the phase boundaries are well established with very small uncertainty. The steady-state fluorescence anisotropy of *m*-cresol (Fig. 4A) increased in the presence of liposomes, suggesting that its rotational dynamic is reduced. The intensity-

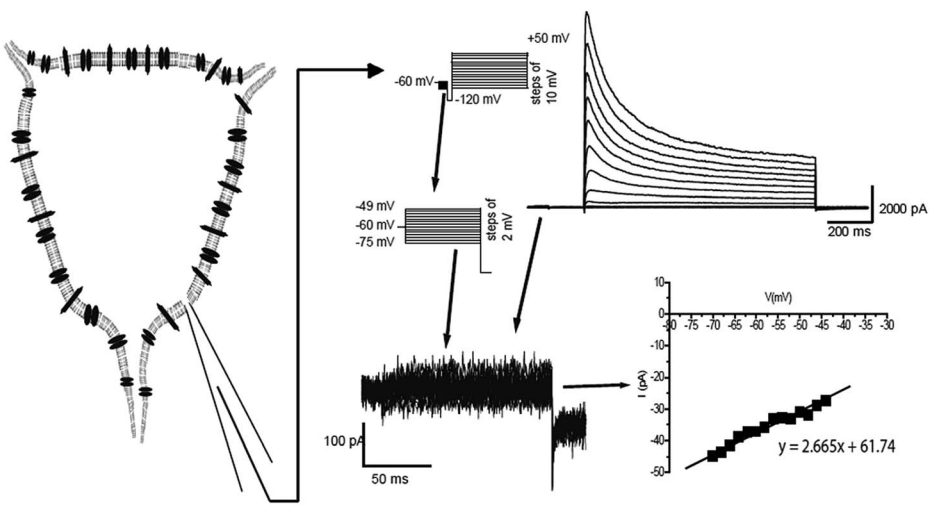

Fig. 2 General scheme illustrating how currents recorded in whole cell voltage clamp are used to estimate leak current. The voltage protocol (see top inset) included two sets of incremental steps. The command pulses with 10 mV step increments elicited voltage activated (K^+) currents only at potentials greater than −30 mV. The preceding series of steps, with small increments, did not evoke any voltage activated current (see currents below). The consequent current–voltage relationship shows a linear tendency that reports leak current only.

weighted average fluorescence lifetime (Fig. 4B), which is proportional to the steady-state fluorescence intensity, follows the same trend, confirming that *m*-cresol mobility is in fact reduced as a result of the interaction with liposomes and that the microenvironment of the molecule is significantly changed. Furthermore, this interaction depends on the membrane lipid composition, since the values tend to decrease as the content in PSM/Chol becomes higher. This could indicate that *m*-cresol may interact more strongly with disordered domains. However, the shape of both curves suggests that the interaction of *m*-cresol with ordered domains should be preferred, because small fractions of l_o are sufficient to induce a noticeable change in the photophysical parameters of *m*-cresol. When the gel phase is present instead of the liquid ordered phase (Fig. S1†), the intensity-weighted average fluorescence lifetime values of *m*-cresol do not show a distinct preference for the lipid phase, since the shape of the curve does not exhibit the same trend to what is observed in the presence of the liquid ordered phase. Regarding Humulin®, since it is composed of two species with intrinsic fluorescence properties, insulin and *m*-cresol, anisotropy values obtained should be the weighted sum of the individual anisotropies of these two fluorophores, by anisotropy additivity law:[28]

$$r_{\text{Humulin}} = f_{\text{insulin}} r_{\text{insulin}} + f_{m\text{-cresol}} r_{m\text{-cresol}} \quad (5)$$

where r is the anisotropy value and f is the fractional intensity. The fractional intensity of each species depends on its molar fraction and fluorescence quantum yield. Since insulin fluorescence emission is mainly due to the four tyrosine residues, an amino acid residue with an aromatic group,[34] and *m*-cresol is a phenolic compound, the quantum yield of each species should be similar. Thus, the difference between the *m*-cresol and insulin contributions to Humulin® anisotropy is mainly due to their molar fraction. It is known that in the Humulin® formulation, the molar concentration of *m*-cresol is *ca.* 38-fold higher than the insulin concentration (Eli Lilly and Company), which explains why anisotropy values obtained for *m*-cresol are comparable to the ones obtained for Humulin (Fig. 4C). As a result of its larger hydrodynamic volume, insulin's anisotropy value in the presence of liposomes is also much larger than *m*-cresol's anisotropy values (*ca.* 0.06), and it does not change (data not shown) with the lipid composition.

Additionally, the Humulin® steady-state anisotropy (Fig. 4C) and intensity-weighted mean fluorescence lifetimes (Fig. 4D) exhibit the same behaviour as pure *m*-cresol in the presence of ternary lipid bilayers (Fig. 4A and B), increasing with the same dependency on the lipid phase. These results show that *m*-cresol in Humulin® formulation is also able to interact with the membrane. Upon an increase of *m*-cresol concentration, anisotropy and intensity-weighted mean fluorescence lifetime values slightly decrease, indicating that with the increase in *m*-cresol concentration, the system becomes more complex and a simple membrane/water partition of *m*-cresol is not sufficient to quantitatively describe the data.

Interactions of *m*-cresol with biomembranes evaluated through membrane fluorescent probes

The highly-used excipient *m*-cresol is able to interact with models of the mammalian plasma membrane outer leaflet, both alone and when present in an insulin formulation used for human diabetes therapy. Thus, it can be anticipated that the interaction of *m*-cresol, both alone and in the formulation, may have effects on membrane lipid organization/biophysical properties. Thus, to fully characterise these interactions, it was necessary to label liposomes with several membrane probes spanning a range of in-depth locations and with preferences for

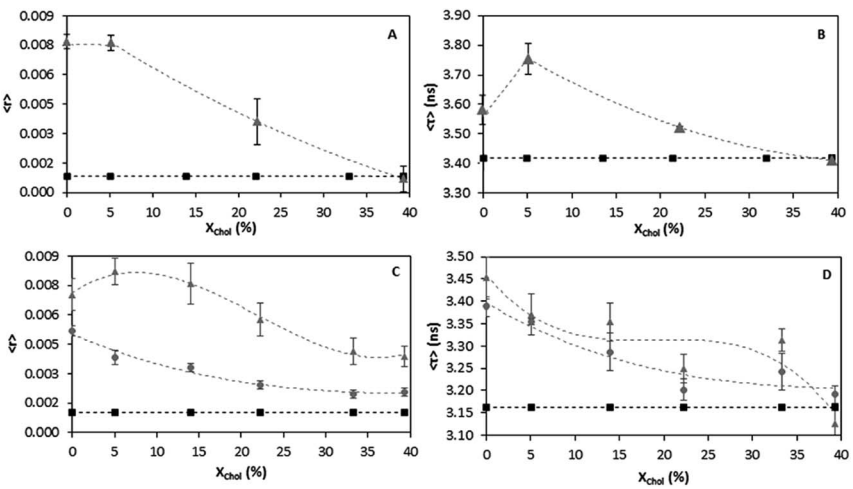

Fig. 4 Steady-state fluorescence anisotropy (A) and intensity-weighted average fluorescence lifetime (B) of pure *m*-cresol at 30 μM. Both measurements were performed in the absence (squares) and presence of LUV (ternary mixtures of POPC/PSM/Chol with molar proportions as indicated in Materials and methods) (triangles). Steady-state fluorescence anisotropy (C) and intensity-weighted average fluorescence lifetime (D) of Humulin® containing *m*-cresol at 100 μM (triangles) and 1 mM (circles). Both measurements were also performed in the absence of LUV (squares). The values are the mean ± standard deviation of at least 3 independent experiments. The dotted lines are merely guides for the eye. All experiments were performed at room temperature.

distinct lipid domains and biophysical properties (*e.g.* ref. 35–37). Two different head-labelled phospholipid analogues localised at the membrane interface[38] were used, NBD-DPPE, which partitions preferentially into the l_o phase,[21,39] and NBD-DOPE, which partitions preferentially into l_d phases.[40] Upon addition of *m*-cresol, both NBD-DPPE (Fig. 5A) and NBD-DOPE (Fig. 5B) intensity-weighted average fluorescence lifetimes decreased, indicating that *m*-cresol locates preferentially, at least in a first stage, at the membrane surface of both ordered and disordered domains. Moreover, this interaction should preferentially affect disordered domains, since the magnitude of the variation is smaller in the case of NBD-DPPE (Fig. 5A) and the amplitude-weighted mean fluorescence lifetime values follow the same trend with and without the presence of *m*-cresol.

In order to understand if *m*-cresol effects are restricted to the membrane surface or if it also interacts with the hydrophobic core of the lipid bilayer, the intensity-weighted mean fluorescence lifetime of the probe *trans*-parinaric acid (*t*-PnA) was measured in the presence of *m*-cresol. *t*-PnA is a very useful probe to assess even subtle changes in the organization of ordered lipid domains, both in membrane model systems[41,42] and in living cell membranes.[36,43] In addition, it provides information about the packing of phospholipid acyl chains, since its chromophore is integrated inside the bilayer core.[44] The intensity-weighted average fluorescence lifetime of *t*-PnA (Fig. 6) does not seem to be affected by the presence of *m*-cresol, not even when its concentration increases 10-fold. Interestingly, the intensity-weighted average fluorescence lifetime of *t*-PnA, which is already longer in l_o,[41] becomes slightly longer. Rather than leading to a decreased packing in the more ordered and compact l_o domains, as could be intuitively expected, it seems to have an opposite effect. The major conclusion is, however, that the effects of *m*-cresol on membranes do not occur at the hydrophobic core level and it only adsorbs onto the surface, probably involving H-bonding of the phenol OH group with the lipid headgroups.

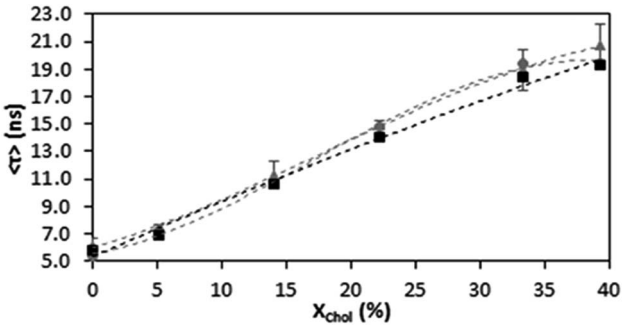

Fig. 6 Intensity-weighted average fluorescence lifetime of *t*-PnA in the absence (squares) and presence of *m*-cresol at 30 μM (circles) and 300 μM (triangles). Both experiments were performed in LUV of ternary mixtures of POPC/PSM/Chol, with molar proportions as indicated in Materials and methods, at room temperature. The values are the mean ± standard deviation of at least 3 independent experiments. The dotted lines are merely guides for the eye.

Interactions of *m*-cresol with liquid ordered domains evaluated in real-time by AFM

As previously shown by fluorescence spectroscopy, the effects of *m*-cresol on the lipid bilayer seem to be restricted to its surface and are dependent on the lipid phase. To clarify these effects, *in situ* tapping-mode AFM was performed to follow real-time detailed morphological and structural changes induced by *m*-cresol on SLB. For that purpose, ternary mixtures of DOPC/PSM/Chol with a molar ratio of 40/40/20 were used to form SLB

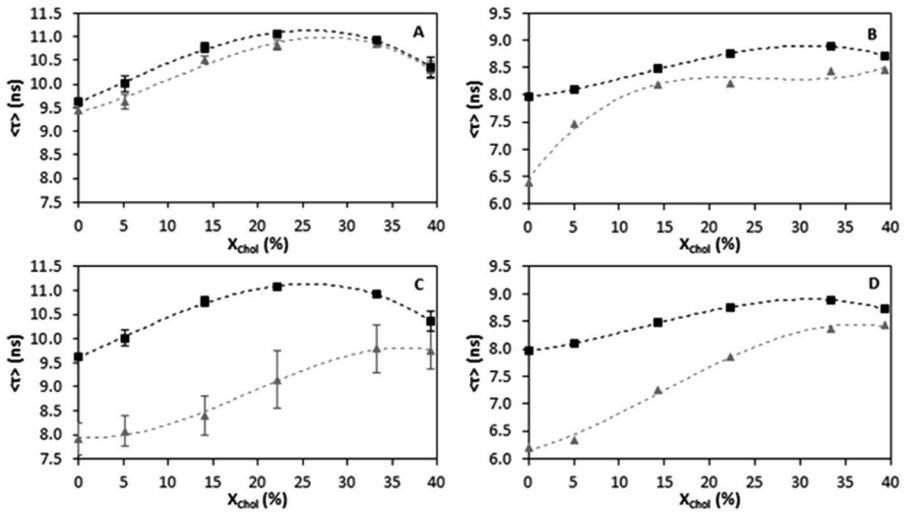

Fig. 5 Intensity-weighted average fluorescence lifetime of NBD-DPPE in the absence (squares) and presence (triangles) of pure *m*-cresol at 30 μM (A) and *m*-cresol at 100 μM from Humulin® (C); intensity-weighted average fluorescence lifetime of NBD-DOPE in the absence (squares) and presence (triangles) of pure *m*-cresol at 30 μM (B) and *m*-cresol at 100 μM from Humulin® (D). Both measurements were performed in the presence of LUV (ternary mixtures of POPC/PSM/Chol with molar proportions as indicated in Materials and methods) at room temperature. The values are the mean ± standard deviation of at least 3 independent experiments. The dotted lines are merely guides for the eye.

containing raft-like PSM/Chol-enriched l_o domains on mica (Fig. 7). The DOPC-containing mixture is better suited for studying membrane lipid organization by AFM, since the l_o domains formed have higher height contrast and better definition, allowing a more reliable detection and quantification of these nanodomains.[45] According to the lipid phase diagram,[46] by using this lipid proportion at room temperature, two liquid phases are assembled, with both PSM and Chol preferentially localised in the l_o phase (thicker), surrounded by DOPC in the l_d phase (thinner).[47] In the absence of *m*-cresol (Fig. 7A), coexistence of l_o and l_d domains in the predicted proportions[48] is evident and the thickness gap between them is close to 1 nm (Table 1, Fig. 7), as previously reported.[25] Upon addition of *m*-cresol, a gradual decrease in the size and number of small l_o domains is observed (Fig. 7). Both effects are clearly depicted in the circles, for *m*-cresol at 300 μM concentration. Despite that, the l_d phase remains apparently unchanged with no detectable thickness variation (Table 1, Fig. 7). For higher *m*-cresol concentrations (successive addition), the reduction in small l_o domains is even clearer and the l_o fraction tends to decrease concomitantly with an increase of the l_d fraction. Upon *ca.* two hours exposure of the SLB to the highest *m*-cresol concentration (3 mM), l_o domains totally disappear (Fig. 7E), meaning that the effects of *m*-cresol are both time and concentration-dependent. In fact, these effects on the SLB are undoubtedly caused by *m*-cresol interaction, since scanning the surface repeatedly does not significantly change the domain morphology (Fig. S2†). The same experiments were performed with the addition of Humulin® containing the same range of *m*-cresol concentrations (Fig. 8). On the whole, Humulin® promotes a progressive disruption of the SLB l_o domains, as observed in the presence of *m*-cresol. These effects should be a consequence of an interaction with l_o/l_d boundaries, since first they lead to the disappearance of small l_o domains and then to the entire l_o fraction. Interestingly, for each *m*-cresol concentration, the percentage of l_o reduction is lower after the addition of Humulin® than when pure *m*-cresol is added. For example, after addition of Humulin® containing *m*-cresol at 300 μM, only 8% of the l_o fraction is lost (Table 1), but in the presence of the same concentration of pure *m*-cresol, the l_o fraction is reduced by 11%. Moreover, in the presence of pure *m*-cresol at 3000 μM, all of the l_o fraction is converted into l_d fraction (Table 1) and, in the presence of Humulin® containing *m*-cresol at a concentration 10-fold higher (3 mM), the l_o fraction was reduced only by 46%. These results show that *m*-cresol, *per se*, affects membrane lateral organization in a more damaging way than when it is contained in Humulin®.

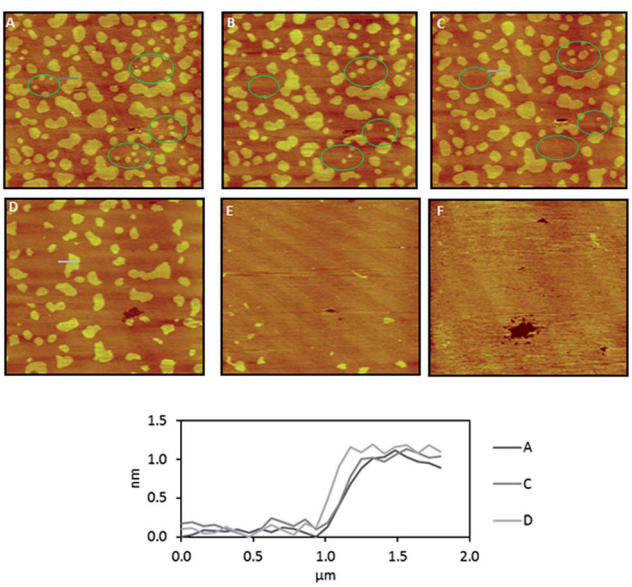

Fig. 7 *m*-Cresol interaction with a bilayer displaying l_d/l_o phase separation on mica. AFM images of an SLB composed of DOPC/PSM/Chol (40/40/20 mol/mol/mol) deposited on mica, in the absence of *m*-cresol (A), 1 h (B) and 2 h (C) after the addition of *m*-cresol at 300 μM, and 5 min (D), 1 h (E) and 2 h (F) after the addition of *m*-cresol at 3 mM in HEPES buffer. Circles show changes in the shape of l_o domains after addition of *m*-cresol. The inset shows the topographical profiles corresponding to the grey lines in panels A, C and D. The images were obtained in a liquid cell at room temperature. The images correspond to an area of 20 × 20 μm^2. $Z = 5$ nm.

Interaction of *m*-cresol with neuronal cell membrane evaluated by leak current

To deduce possible consequences of the results above at a cellular level, a study of the effects of *m*-cresol on cell membrane passive permeability was carried out by monitoring leakage current using the whole cell voltage clamp approach (Fig. 2). In Fig. 9, *I*/*V* data are presented for the isolated CA1 pyramidal neurons. A similar nature of effects and patterns evoked by *m*-cresol were found for small diameter DRG neurons and for N1E-115 cells. The results obtained for leak conductance changes are presented in Fig. 10. Fig. 9 shows the effects of *m*-cresol on passive leak current. Two examples are presented, both obtained from CA1 pyramidal neurons, in each of which two different concentrations were used. From Fig. 9A, one can observe from the time course that *m*-cresol at 3 μM does not evoke any alteration in the holding current ($V_m = -70$ mV). Also, the chord leak conductance remains unaltered. If anything, the leakage became slighter smaller throughout the experiment, as is usually the case in such recordings (see control bars in Fig. 10). In contrast, Fig. 9B shows a clear effect of *m*-cresol at a greater concentration (300 μM). By observing the time course, a clear effect of the holding current is seen. In fact, after washing out the *m*-cresol, a slight recovery is obtained, as was observed in some of the experiments. This increase in holding current represents an increase in leak current, as it is due to the feedback system which is set to clamp the potential at −70 mV. To confirm this, we estimated the leakage chord conductance before and during the superfusion of *m*-cresol, at a time point in which the holding current has stabilized. For the case presented, the slope of the fitted linear regression increases 2.7 times, meaning a substantial increase of leak current. Similar experiments to the one presented in Fig. 9 were conducted with different concentrations of *m*-cresol (3, 30, and 300 μM) in hippocampal CA1 neurons (Fig. 10, dark bars). The variation of conductance was compared with control

Table 1 Percentage of reduction of the area occupied by the l_o phase on SLB deposited on mica and height difference between the l_o and l_d phases after addition of both pure *m*-cresol and Humulin®. l_o, liquid ordered; l_d, liquid disordered. Calculations were performed based on AFM topographic images after 2 h exposure to pure *m*-cresol and Humulin®. The values are the mean ± standard deviation of at least 10 different topographic profiles

	Pure *m*-cresol		Humulin®	
[*m*-Cresol] (μM)	l_o area reduction (%)	Domain height difference (nm)	l_o area reduction (%)	Domain height difference (nm)
0	0	1.0 ± 0.2	0	1.2 ± 0.1
3	0	1.0 ± 0.2	0	1.2 ± 0.1
30	9	1.1 ± 0.1	8	1.3 ± 0.1
300	17	0.9 ± 0.1	8	1.3 ± 0.1
3000	100	—	46	1.3 ± 0.1

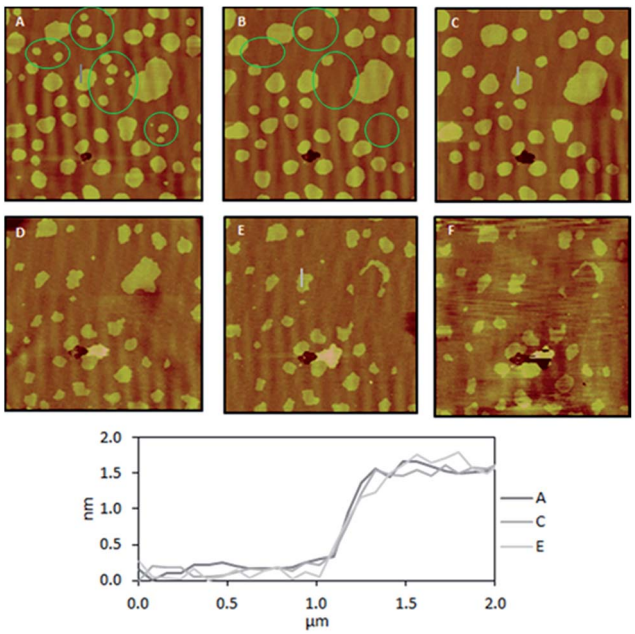

Fig. 8 Humulin® interaction with a bilayer displaying l_d/l_o phase separation on mica. AFM images of an SLB composed of DOPC/PSM/Chol (40/40/20 mol/mol/mol) deposited on mica, in the absence of Humulin® (A), 1 h (B) and 2 h (C) after the addition of Humulin® containing *m*-cresol at 300 μM, and 5 min (D), 1 h (E) and 2 h (F) after the addition of Humulin® containing *m*-cresol at 30 mM in HEPES buffer. Circles show changes in the shape of l_o domains after addition of Humulin®. The inset shows the topographical profiles corresponding to the grey lines in panels A, C and E. The images were obtained in a liquid cell at room temperature. The images correspond to an area of 20 × 20 μm^2. $Z = 7$ nm.

recordings, with no *m*-cresol added (zero *m*-cresol at the *x* axis), values which were taken after 45 minutes of recording. Most importantly, there is a substantial increase of leak conductance only for a *m*-cresol concentration of 300 μM. At 30 μM, there is no response in leak current. Such results were obtained in hippocampal, *i.e.*, central neurons. There was thus interest to investigate if such effects were also observed in other neural cells and, in particular, neurons from the peripheral nervous system. Therefore, Fig. 10 also includes neuroblastoma N1E-115 cells (patterned bars) and small diameter dorsal root ganglia neurons, key in nociception and pain signalling. Most noticeably, the data follow the same pattern and the concentration threshold for the *m*-cresol effect appears to be the same as the one found in hippocampal neurons.

Discussion

The current work presents a detailed study of the effects of an excipient highly used in pharmaceutical formulations, *m*-cresol, on lipid bilayers mimicking the outer leaflet of mammalian plasma membranes. For that purpose, fluorescence spectroscopy and AFM were applied to study the effects of this compound on lipid model membranes composed of binary and ternary mixtures displaying different phase coexistence situations. The experiments were performed with pure *m*-cresol and compared with Humulin®, an example of a commercial pharmaceutical formulation containing *m*-cresol, showing that when this excipient is incorporated in a formulation, its effects are still detectable. The electrophysiological relevance of the effects of *m*-cresol was investigated by conducting recordings in three neuronal cell types, measuring leak current as a read-out of membrane integrity. The data point out a dose-dependent effect on membrane passive permeability, which is consistent with the concentration dependence of the effects observed using membrane model systems.

For the first time, the steady-state fluorescence anisotropy of *m*-cresol (Fig. 4A) and its intensity-weighted average fluorescence lifetime (Fig. 4B) were measured. We demonstrated that the intrinsic fluorescence of *m*-cresol is a valid tool to study the dynamics of *m*-cresol and its interaction with biomembrane models, namely lipid bilayers. Through these measurements, it was unequivocally shown that *m*-cresol interacts with lipid bilayers. Through steady-state fluorescence anisotropy it was shown that, in the presence of liposomes, the mobility of *m*-cresol is more restricted than in the aqueous medium. Intensity-weighted average fluorescence lifetime results show a decrease in the number of collisions between *m*-cresol and water molecules or buffer ions and, at the same time, a reduction in polarity of the medium in the presence of liposomes, which by itself may have an influence on the fluorescence properties of *m*-cresol. Moreover, a less polar environment may prevent the formation of dimers or clusters between different *m*-

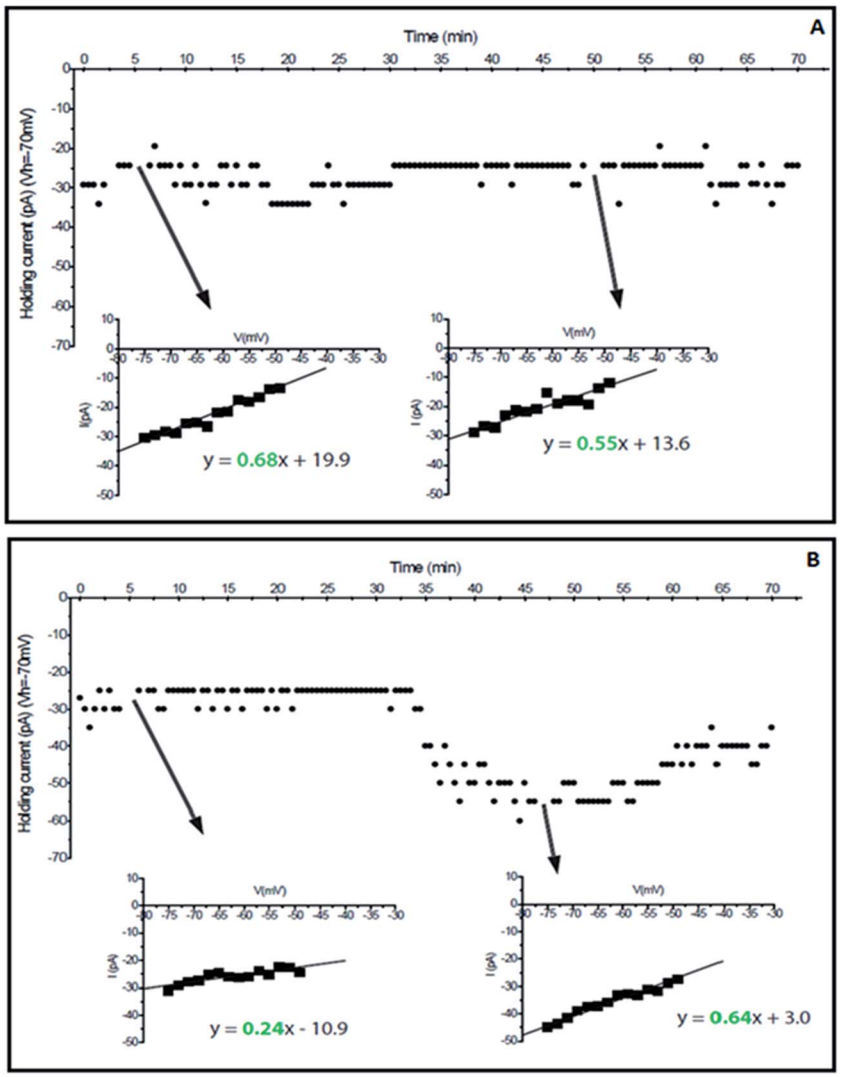

Fig. 9 Whole cell voltage clamp recordings from CA1 pyramidal neurons. (A) Representative experiment with time course of holding current (holding voltage of −70 mV) with superfusion of *m*-cresol at 3 μM. Arrows indicate time points in which voltage protocols (same as presented in Fig. 2) were applied with the consequent calculated *I*/*V* relationships and linear regressions. (B) Represents a similar experiment but with higher *m*-cresol concentration (300 μM).

cresol molecules and therefore the probability of occurrence of self-quenching will be smaller than that in aqueous medium without the presence of liposomes.

Another important hallmark of *m*-cresol is the distinct behaviour in the presence of distinct lipid phases, showing that the biophysical properties of these phases play an important role in the interaction. It seems that the l_d phase is more affected by *m*-cresol than the l_o phase, in which steady-state fluorescence anisotropy (Fig. 4A) and intensity-weighted average fluorescence lifetimes (Fig. 4B) exhibit smaller values. Nevertheless, this result does not mean that in the presence of the l_o phase *m*-cresol does not interact with the bilayer and the small values obtained may be due to energy homo-transference between *m*-cresol molecules, which is enabled by the parallel alignment of the dipolar moments in this lipid phase, and self-quenching phenomena, respectively. These possibilities can occur when *m*-cresol molecules are located at the membrane surface between phospholipid head groups and they are close enough to allow the occurrence of these phenomena. This explanation is corroborated by the results obtained with the NBD-labelled lipids (Fig. 5), since the observed intensity-weighted average fluorescence lifetime decrease can be caused by dynamic self-quenching or by the hydration increase at the bilayer core. The results obtained with *t*-PnA (Fig. 6) suggest then that *m*-cresol should act preferentially on the membrane surface and not at the hydrophobic core level, and the decrease of the intensity-weighted average fluorescence lifetime is only explained by dynamic self-quenching phenomena.

The observation, by AFM, of the effects of *m*-cresol on SLB showed a prominently preferential interaction with l_o/l_d domain boundaries (Fig. 7) in such a way that leads to a progressive reduction of the size of PSM/Chol-enriched nanodomains over time and, for higher concentrations, to the elimination of the ordered phase. Once again, this observation is confirmed by the

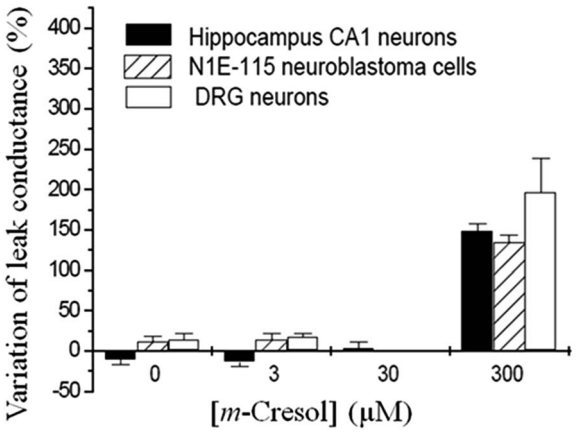

Fig. 10 Pulled data from whole-cell voltage clamp experiments similar to those presented in Fig. 9. Several *m*-cresol concentrations were used. The values are the mean ± standard deviation of at least 3 independent experiments.

results from fluorescence spectroscopy with NBD probes (Fig. 5), indicating that the effects of *m*-cresol are related essentially with an alteration in lipid phase proportions and the size of the l_o domains. Additionally, results obtained from FRET experiments (Fig. S3†) are in agreement with this behaviour, since FRET efficiency between the donor, localized in the l_o phase, and the acceptor, with a preference for the l_d phase, decreases in the presence of *m*-cresol. This result is in agreement with what is expected, since an average increase of the size of the l_o domains results in phase separation and therefore in an increase in donor–acceptor distance, as reported.[21,40] Fluorescence spectroscopy measurements with the lipid mixture composed of DOPC/PSM/Chol, which was used in the AFM studies, were also carried out. The results are in agreement with those obtained with the POPC/PSM/Chol system (Fig. 4–6), regarding both the behaviour of *m*-cresol and the biophysical properties reported using the several fluorescent probes (Fig. S4†).

Globally, the interaction of *m*-cresol with lipid bilayers should involve an initial interaction with the bilayer surface of both the l_o and l_d phases through hydrogen bonds between the OH group of *m*-cresol and the phospholipid head groups. This effect should be restricted to the bilayer surface, without perturbation of the packing of the phospholipid acyl chains. Since the membrane dipole potential is higher in the l_o phase,[49] in this phase the dipolar moment of *m*-cresol aligns with the membrane dipole. Thus, *m*-cresol insertion into an ordered bilayer is energetically compensated by the interaction of dipolar moments. This interaction is the explanation for the *m*-cresol preference for the l_o phase. The packing of this phase is not perturbed during the interaction since *m*-cresol locates preferentially at the membrane surface, aligned with the planar structure of the sterol rings. However, since new hydrogen bonds with *m*-cresol are formed, the sterol–phospholipid hydrogen bonds are replaced, contributing to the further l_o phase destabilization. This superficial interaction should happen preferentially at the interfaces between the l_o and l_d domains, probably because kinetically it is more easy, leading to the disappearance of the small l_o domains and to a progressive reduction of the size of the l_o domains. This change in bilayer organization can be described as a displacement of the ternary mixture phase diagram in the direction of the disordered phase or a shift to higher temperatures. At the final stage, the bilayer should correspond to a disordered phase, but with distinct properties from the initial l_d phase, since it contains large amounts of Chol. In the l_d phase, hydrophobic interactions should avoid contact of *m*-cresol with water molecules, but the orientational freedom will be higher than before, when the membrane was more ordered. Globally, at this stage, the interactions will not be as strong as those with the l_o phase, since there are no specific dipolar interactions between *m*-cresol and the bilayer. This behaviour, based on the interaction of dipolar moments, is similar to the one described to explain the different solubility of two fluorescent lipid probes containing comparable nonpolar structures and different polar head groups, NBD-hexadecylamine and RG-tetradecylamine.[50]

Knowing that in the Humulin® formulation, *m*-cresol concentration is *ca.* 38-fold higher than that of insulin, it was also convenient to study the effects of this formulation on membrane mimetic models under similar conditions to those used for pure *m*-cresol. The results obtained are in agreement with the behaviour of *m*-cresol, suggesting that the cytotoxic effects of Humulin® are largely triggered by *m*-cresol. The toxicity level of *m*-cresol was recently tested and compared to insulin solutions containing *m*-cresol as an excipient.[18] The results revealed that *m*-cresol displays the same level of cytotoxicity as the commercial insulin formulations, whereas insulin solutions without excipients did not cause cell death. Besides that, since *m*-cresol is also a preservative agent, the fact that the trend in intrinsic fluorescence is similar for pure *m*-cresol (Fig. 4A and B) and Humulin® (Fig. 4C and D) is already quite surprising. This conclusion is based on the fact that, in formulation, *m*-cresol may interact with insulin itself and possibly with other components such as glycerol and hence, a more complex trend in the data should be expected. Actually, the system has a large number of components and, for example, a simple membrane/water partition of *m*-cresol is not sufficient to quantitatively describe the data. This is a problem regarding the study of this formulation using cells, since it is not possible to predict whether effects detected are due to *m*-cresol or insulin. This occurs because cells have innumerous receptors for insulin and thus, the application of Humulin® would lead to activation of regulation pathways that will not be activated in the presence of *m*-cresol alone. Therefore, this kind of study has to be performed using model systems, like the one presented here.

In addition, the leak current in living neurons is affected by *m*-cresol at 300 μM concentration (Fig. 9 and 10). Most interestingly is that such effects are transversal, *i.e.* they were observed not only in neuroblastoma cells, but also in key neurons, from both the peripheral and central nervous systems. This universality strongly supports the view that the main effects of *m*-cresol occur at the level of the lipid bilayer. Moreover, since the outer leaflet of mammalian cell membranes,

particularly in the case of neurons, is sphingolipids and Chol-enriched, it is believed to be close to a liquid ordered phase.[51] These ordered domains prevent the interaction and/or strong reorganization of the lipid bilayer induced by small external molecules. However, in the case of *m*-cresol, the studies using lipid mixtures indicate that it in fact has a preference for those liquid ordered phases, which is corroborated by the effects observed in the neuronal membrane. Hence, those results are clearly complementary to establish the physicochemical principles underlying the biological action of small amphiphilic molecules with biomembranes, in this case the toxicological effects of *m*-cresol. We present evidence that the PSM/Chol-enriched domains are strongly affected by *m*-cresol. A recent study pointed out free radical intermediate formation from the oxidation of phenolic compounds, such as *m*-cresol, as a cause of oxidative stress and inflammatory response generation that may lead to cell death.[18] Before that, alterations in membrane fluidity and permeability by means of the increase of lipid peroxidation had been also correlated with the effects of cresol.[11] However, the effects reported here are a result of the direct interaction of *m*-cresol with the plasma membrane. In the case of neuronal membranes, the leakage current increase is observed immediately after the addition of *m*-cresol to the perfusion medium, before peroxidation events have significantly affected membrane permeability. This means that the adsorption of the phenolic compound to the lipid bilayer induces measurable changes in its organization, which can be correlated with the changes observed in the model systems using both AFM and fluorescence. This also means that the effects of this direct interaction can trigger stress responses, that will in turn lead to additional toxic effects, as described by other authors.[11,18] It should also be noted that the regulation of many signalling pathways is linked to the PSM/Chol-enriched domains[52] which are strongly affect by *m*-cresol. The fact that deregulation of several signalling pathways was implied as a mechanism behind the adverse effects of *m*-cresol[18] supports this interpretation. Further metabolization of *m*-cresol once inside the cell will lead to other effects, such as lipid peroxidation and associated inflammatory process.

The alterations in the cell membrane are likely to lead to upstream cellular events, for example in the performance of neurons which, in turn, may trigger unpredictable symptoms. Although the concentration of *m*-cresol reaching central neurons after administration of a *m*-cresol-enriched formulation may be lower than the threshold-concentration found, that may not be the case when we consider DRG neurons, located at the periphery. Also, it would be important to investigate the long term effects brought on by sustained administration habits. The results revealed here are of medical importance since *m*-cresol is present in pharmaceutical formulations already on the market and Humulin® particularly is a widely used drug formulation prescribed as an adjunct to diet and exercise for patients with type 1 and type 2 diabetes mellitus. Furthermore, Humulin® administration may be done subcutaneously or through intravenous injection. Thus, a fast release of formulation components leads to a fast spread of *m*-cresol over the body, including blood circulation and contact with cells, especially with cell membranes. Once in contact with the outer leaflet of the plasma membrane, it may act on membrane constituents, *via* mechanisms described here, with possible implications in intracellular signaling pathways.[18] As a matter of fact, some of the skin irritation cases reported[4] using insulin-pump therapy containing *m*-cresol may be due to the effects of *m*-cresol described here. Hence, this study will certainly contribute to unravelling the mechanisms of toxicity of pharmaceutical formulations containing *m*-cresol, like insulin preparations, at the membrane level.

Conclusions

In this work , we present a detailed biophysical study on *m*-cresol–biomembrane interactions using membrane model systems selected to mimic the outer leaflet of human plasma membranes and, particularly, cholesterol-sphingomyelin enriched mixtures, and neuronal cells. It was clearly demonstrated that this excipient alters the passive permeability of neuronal cells and interacts with lipid membranes, leading to their lipid domain reorganisation. A preference for the l_o phase, explained by the interaction between the *m*-cresol dipole and bilayer dipole potential, was identified by fluorescence measurements and visualized in real-time by AFM. A similar behaviour was observed in the presence of *m*-cresol contained in Humulin®, whose side effects have been reported. Such a preference for a more ordered phase, which usually excludes impurities and xenobiotics, might be invoked to explain the interaction of other similar compounds with human cell membranes, which are highly enriched in sphingolipids and cholesterol, and are currently believed to be mostly in a liquid ordered-like state. A wide range of *m*-cresol concentrations, from its value in insulin formulations down to several orders of magnitude below, was used. The purpose was to disclose the effects of *m*-cresol on the membranes of cells located at the site of application, which can potentially be subject to its original concentration in the formulation, and those that are more distant from the injection site, but still vulnerable to the effects of lower concentrations of *m*-cresol. Thus, additional clues are provided here to reveal some of the possible causes for the cytotoxic effects of *m*-cresol and consequently parenteral formulations containing this excipient. Once again, the cell membrane, being the first barrier to entrance into cells, arises as a determinant aspect for understanding the mechanisms behind the action of small amphiphilic compounds of biological and medical relevance.

Acknowledgements

This work was financed by Portuguese national funds through FCT: PEst 2015–2020 (UID/Multi/00612/2013), PTDC/BBB-BQB/6071/2014, PTDC/CTM-NAN/0994/2014, IF/00808/2013/CP1159/CT0003 including fellowships to J. T. M. and T. O. P., A. E. P. B. doctoral scholarship SFRH/BD/88199/2012 and IF 2012/2013 initiatives (POPH, Fundo Social Europeu).

References

1 H. Fiege, in *Ullmann's Encyclopedia of Industrial Chemistry*, Wiley-VCH Verlag GmbH & Co. KGaA, Weinheim, Germany, 2012, vol. 10, pp. 419–461.
2 D. C. Thompson, K. Perera, R. Fisher and K. Brendel, *Toxicol. Appl. Pharmacol.*, 1994, **125**, 51–58.
3 M. C. Chang, H. H. Chang, C. P. Chan, S. Y. Yeung, H. C. Hsien, B. R. Lin, C. Y. Yeh, W. Y. Tseng, S. K. Tseng and J. H. Jeng, *PLoS One*, 2014, **9**, e114446.
4 I. van Faassen, P. P. Razenberg, A. M. Simoons-Smit and E. A. van der Veen, *Diabetes Care*, 1989, **12**, 153–155.
5 I. van Faassen, A. M. Verweij-van Vught, M. Z. Lomecky-Janousek, P. P. Razenberg and E. A. van der Veen, *Diabetes Care*, 1990, **13**, 71–74.
6 Y. Kamijo, K. Soma, M. Kokuto, M. Ohbu, C. Fuke and T. Ohwada, *Arch. Pathol. Lab. Med.*, 2003, **127**, 364–366.
7 Cresol (*o*, *m*, *p* isomers), http://www.cdc.gov/niosh/idlh/cresol.html, accessed June 2016.
8 Agency for Toxic Substances and Disease Registry, *Toxicological Profile for Cresols*, Public Health Service, U.S. Department of Health and Human Services, Atlanta, GA, 1990.
9 S. Fujisawa, Y. Kadoma and E. Masuhara, *J. Biomed. Mater. Res.*, 1987, **21**, 89–98.
10 H. W. Jeng, R. J. Feigal and H. H. Messer, *Pediatr. Dent. J.*, 1987, **9**, 295–300.
11 D. Calderon-Guzman, J. L. Hernandez-Islas, I. R. Espitia Vazquez, G. Barragan-Mejia, E. Hernandez-Garcia, D. S. Del Angel and H. Juarez-Olguin, *Regul. Toxicol. Pharmacol.*, 2005, **41**, 1–5.
12 B. J. Lewis, *J. Calif. Dent. Assoc.*, 2010, **38**, 102–107.
13 R. Tisserand and R. Young, in *Essential Oil Safety: A Guide for Health Care Professionals*, Churchill Livingstone, 2nd edn, 2014.
14 M. F. Dunn, *Biometals*, 2005, **18**, 295–303.
15 J. Brange and L. Langkjaer, *Acta Pharm. Nord.*, 1992, **4**, 149–158.
16 A. M. Gualandi-Signorini and G. Giorgi, *Eur. Rev. Med. Pharmacol. Sci.*, 2001, **5**, 73–83.
17 H. Eriksson, *Biotechnol. Tech.*, 1998, **12**, 329–334.
18 C. Weber, D. Kammerer, B. Streit and A. H. Licht, *Toxicol. Rep.*, 2015, **2**, 194–202.
19 National Center for Biotechnology Information, PubChem Compound Database, https://pubchem.ncbi.nlm.nih.gov/compound/342, accessed June 2016.
20 R. F. M. de Almeida, A. Fedorov and M. Prieto, *Biophys. J.*, 2003, **85**, 2406–2416.
21 R. F. M. de Almeida, L. M. Loura, A. Fedorov and M. Prieto, *J. Mol. Biol.*, 2005, **346**, 1109–1120.
22 C. W. McClare, *Anal. Biochem.*, 1971, **39**, 527–530.
23 I. B. Berlman, in *Handbook of Fluorescence Spectra of Aromatic Molecules*, ed. I. B. Berlman, Academic Press, 2nd edn, 1971, pp. 67–95.
24 I. S. Johnson and M. T. Z. Spence, *Molecular Probes Handbook, A Guide to Fluorescent Probes and Labeling Technologies*, Molecular Probes, Eugene, OR, USA, 11th edn, 2010.
25 J. T. Marquês, A. S. Viana and R. F. M. de Almeida, *Biochim. Biophys. Acta*, 2011, **1808**, 405–414.
26 L. D. Mayer, M. J. Hope and P. R. Cullis, *Biochim. Biophys. Acta*, 1986, **858**, 161–168.
27 E. Zupancic, A. C. Carreira, R. F. M. de Almeida and L. C. Silva, *J. Phys. Chem. B*, 2014, **118**, 4858–4866.
28 J. R. Lakowics, *Principles of Fluorescence Spectroscopy*, Springer, New York, 3rd edn, 2006.
29 L. M. Loura, R. F. M. de Almeida, L. C. Silva and M. Prieto, *Biochim. Biophys. Acta*, 2009, **1788**, 209–224.
30 M. I. Vicente, P. F. Costa and P. A. Lima, *Eur. J. Pharmacol.*, 2010, **634**, 16–25.
31 S. A. Malin, B. M. Davis and D. C. Molliver, *Nat. Protoc.*, 2007, **2**, 152–160.
32 H. B. Wang, Y. J. Zhang, X. Xiao, D. Jin, N. J. Zhao, G. F. Yin, L. Q. Guo and W. Q. Liu, *Spectrosc. Spectral Anal.*, 2010, **30**, 1271–1274.
33 G. Garbes Putzel and M. J. Schick, *J. Phys.: Condens. Matter*, 2011, **23**, 284101.
34 J. P. Mayer, F. Zhang and R. D. DiMarchi, *Biopolymers*, 2007, **88**, 687–713.
35 A. Khmelinskaia, M. Ibarguren, R. F. M. de Almeida, D. J. Lopez, V. A. Paixao, H. Ahyayauch, F. M. Goni and P. V. Escriba, *Langmuir*, 2014, **30**, 2117–2128.
36 A. E. Bastos, H. S. Marinho, A. M. Cordeiro, A. M. de Soure and R. F. M. de Almeida, *Chem. Phys. Lipids*, 2012, **165**, 577–588.
37 J. T. Marquês, C. A. C. Antunes, F. C. Santos and R. F. M. de Almeida, in *Advances in Planar Lipid Bilayers and Liposomes*, ed. C. V. K. Aleš Iglič and R. Michael, Academic Press, 2015, vol. 22, pp. 65–96.
38 S. Mukherjee, H. Raghuraman, S. Dasgupta and A. Chattopadhyay, *Chem. Phys. Lipids*, 2004, **127**, 91–101.
39 C. Dietrich, L. A. Bagatolli, Z. N. Volovyk, N. L. Thompson, M. Levi, K. Jacobson and E. Gratton, *Biophys. J.*, 2001, **80**, 1417–1428.
40 B. M. Castro, R. F. M. de Almeida, E. Goormaghtigh, A. Fedorov and M. Prieto, *Biophys. J.*, 2011, **101**, 1632–1641.
41 L. A. Sklar, B. S. Hudson and R. D. Simoni, *Biochemistry*, 1977, **16**, 819–828.
42 R. F. M. de Almeida, L. M. Loura and M. Prieto, *Chem. Phys. Lipids*, 2009, **157**, 61–77.
43 F. Aresta-Branco, A. M. Cordeiro, H. S. Marinho, L. Cyrne, F. Antunes and R. F. de Almeida, *J. Biol. Chem.*, 2011, **286**, 5043–5054.
44 M. Castanho, M. Prieto and A. U. Acuna, *Biochim. Biophys. Acta*, 1996, **1279**, 164–168.
45 J. V. Bleecker, P. A. Cox, R. N. Foster, J. P. Litz, M. C. Blosser, D. G. Castner and S. L. Keller, *J. Phys. Chem. B*, 2016, **120**, 2761–2770.
46 T. K. Nyholm, D. Lindroos, B. Westerlund and J. P. Slotte, *Langmuir*, 2011, **27**, 8339–8350.
47 C. B. Yuan, J. Furlong, P. Burgos and L. J. Johnston, *Biophys. J.*, 2002, **82**, 2526–2535.

48 R. F. M. de Almeida, J. Borst, A. Fedorov, M. Prieto and A. J. Visser, *Biophys. J.*, 2007, **93**, 539–553.
49 S. Bandari, H. Chakraborty, D. F. Covey and A. Chattopadhyay, *Chem. Phys. Lipids*, 2014, **184**, 25–29.
50 L. M. B. B. Estronca, M. João Moreno, M. S. C. Abreu, E. Melo and W. L. C. Vaz, *Biochem. Biophys. Res. Commun.*, 2002, **296**, 596–603.
51 R. F. M. de Almeida and E. Joly, *Front. Plant Sci.*, 2014, **5**, 72.
52 S. Jin, F. Zhou, F. Katirai and P. L. Li, *Antioxid. Redox Signaling*, 2011, **15**, 1043–1083.